PACEMAKER RHYTHM THROUGH NETWORKS OF PACEMAKER AUTOMATA — A REVIEW*

Danuta Makowiec

Institute of Theoretical Physics and Astrophysics, Gdańsk University
Wita Stwosza 57, 80-952 Gdańsk, Poland
fizdm@univ.gda.pl

(Received March 10, 2014)

Self-organization in biological systems often emerges as widespread oscillatory dynamics of coupled units. Two types of oscillation phenomena can be investigated in networks of automata. One may observe sustained oscillations in a system of non-oscillating automata (as in, *e.g.*, the Greenberg–Hastings cellular automata), or one may investigate synchronization, *i.e.* self-organization of individual cellular oscillations to the common oscillation. Both approaches are used in modeling cardiac electrophysiology. This paper begins with a review of the capabilities and limitations of these propositions in reproducing the functionality of the human pacemaker. Then, an approach to modeling the pacemaker tissue is presented that is based on timed automata having heterogeneous topology of couplings. Timed automata combine intrinsic cellular transitions with nearest neighbor interactions. The complex topology of intercellular interactions is modeled by a stochastic network with the heterogeneous structure arising from the preferential rewiring. The resulting simulation framework exhibits significantly improved computational efficiency in modeling different aspects of the self-organization to the common wave patterns, and furthermore, in reproducing changes in the pacemaker tissue caused by biological aging.

DOI:10.5506/APhysPolBSupp.7.347
PACS numbers: 05.45.Xt, 05.10.–a, 03.20, 45.05.+x

1. Motivation and objectives

Discrete state, space, and time systems have been successfully used in explaining collective phenomena of a thermodynamic type, such as continuous phase transition in ferromagnetic media [1–3], or a dynamical type like self-organized criticality [4]. The cellular automata technique has been

* Presented at the Summer Solstice 2013 International Conference on Discrete Models of Complex Systems, Warszawa, Poland, June 27–29, 2013.

successfully applied in the study of critical phenomena in various fields. Consider, for example, the Nagel–Schreckenberg model of road traffic [5], or the percolation model of imitation and herding on financial markets [6, 7].

However, in biological systems, self-organization mostly emerges as the widespread oscillatory-type dynamics of coupled units [8]. Two types of this kind of collective phenomenon can be investigated within the framework of cellular automata. Firstly, we may observe the emergence of sustained oscillations in the system of non-oscillating units. Secondly, we may study the self-organization of the intrinsic oscillations of each automata to the common oscillation of the system.

The *Greenberg–Hastings* (GH) cellular automata system [9] — the model of so-called excitable media — is a prototype for a system achieving sustained oscillations when the elementary units are not oscillators. But if we replace each automaton with a discrete oscillating element and distribute these elements over some complex network, we then move to a *pacemaker automata network* (PAN), in which the phenomenon of synchronization can be investigated.

When describing the synchronization, one intuitively thinks of the adjustment of rhythms of oscillating objects due to their interactions [8]. In general, this adjustment manifests as the frequency entrainment of oscillators, and if this is the case, phase entrainment synchronization can then emerge. Here, the synchronicity will be investigated in terms of the Kuramoto order parameter [10, 11]. It will be shown that this description provides consistent quantification of stationary states arising from the PAN model considered.

In distinction to the so-called hybrid cellular automata that are based on the close relation of the automata transitions to the continuous models of a cardiac cell [12] (such as *e.g.*, the Hodgkin–Huxley model of the giant squid axon [13] or the Luo–Rudy model of a guinea pig ventricular cell [14]), the approach based on the PAN, focuses on topological aspects of the phenomenon of synchronization, namely on implications of the topology to the synchronization. For this reason, the PAN model not only provides the reconstruction of biochemical properties of the cellular membrane, but also refers to the spatial organization of the cells.

The flexibility of the PAN allows different aspects of modern physiology to be efficiently taken into account. We believe that in this way, the discrete systems offer a valuable tool for explaining qualitatively and sometimes quantitatively properties observed in nature. Moreover, systems biology [15, 16] requires models that bridge different time and space scales, such as the discrete models discussed here.

The GH model is redrafted in Sec. 2 to explain the essentials of self-organization in excitable systems. Some important physiological facts are also presented [17–21], which justify the extension of the GH proposition to the *pacemaker automata network*. In Sec. 3, we introduce the notion of timed automata (based on [22, 23]) and discuss pulse synchronization in a fully connected network of timed automata. The PAN model and a discussion about synchronization under different topological conditions are presented in Sec. 4. Finally, we explain how changes in the human pacemaker, which appear due to aging of the organism, can be examined within the proposed PAN.

2. Emergence of oscillations in GH models

The GH model [24, 25] assumes that vertices of a square lattice are occupied by cells that can be in an *activity* state, denoted as 0, a *firing* state, denoted 1, or in a sequence of recovery states: coded as $2, \ldots, T-1$, when a cell is *refractory* to any interactions. But if a cell is in state 0 and this cell has a sufficient number of neighbors in state 1, it switches to *firing* and then starts the recovery process. With each time step, its state advances from 2 to $T-1$. Finally, the cell's state switches back to the *activity* state, and the cell waits for the next excitation. Thus cellular automata imitate excitable media, *i.e.* media composed of excitable cells but otherwise quiet.

2.1. Sustained oscillations in GH automata on a square lattice

Let us assume that cells are located on the vertices of an $L \times L$ square lattice. Traditionally, two types of cell neighborhood are considered on a square lattice: the von Neumann neighborhood, consisting of four cells connected by horizontal and vertical edges of the lattice, and the Moore neighborhood, in which additionally four cells connected by diagonal edges are included.

Let all cells $J' \in L \times L$ which have a direct connection to J be neighbors of J, which we denote as $J' \in \mathcal{N}(J)$.

Let σ denote the state of a cell, $\sigma \in \{0, 1, \ldots, T-1\}$.

Then, the state of the cellular system at time t is represented by a function

$$\phi(t) : L \times L \to \{0, 1, \ldots, T-1\} \tag{1}$$

that evolves according to the rule:

for any $J \in L \times L$

(I) if $\phi(t, J) = \sigma \geq 1$, then $\phi(t+1, J) = (\sigma + 1) \bmod T$;

(II) if $\phi(t, J) = 0$, then $\phi(t+1, J) = 1$ if more than F of its neighbors are 1, otherwise $\phi(t+1, J) = 0$.

Rule (I) describes the free evolution of a cell. Rule (II) introduces interactions with the nearest neighbors by the cells. F is the threshold for these interactions.

Starting from a random state (called a primordial soup), after many time steps we observe that cellular states are well-organized in patterns. These patterns live independently of each other on the network, though subordinating free cells, *i.e.*, cells not involved in any pattern. They are either stable and periodic, and therefore called *stable periodic oscillations* (SPO) [25], or all the cells reach the same state $\phi(t, J) = 0$; see Fig. 1. It is obvious that for large F, the system reaches the homogeneous state. However, a general classification of the limiting behavior is difficult.

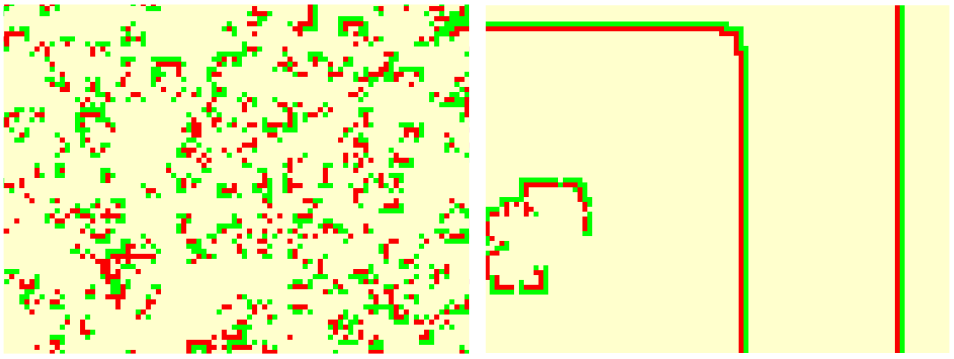

Fig. 1. Examples of the SPO patterns obtained for $F > 0$ and: $T = 9$ (left) and $T = 32$ (right). On the left-hand side, we observe many coexisting SPOs. The pattern in the right plot is driven by one SPO. Such a pattern occurs rarely (with prob. $< 5\%$) for $T = 32$. Cells in the firing state are coded in dark gray/red, active cells are medium gray/green, cells in the refractory state are light gray/yellow.

In the simplest case, the GH system is built from the three-state cellular automata: 0 for the activity, 1 for the firing, and 2 for the refractory. The nearest neighbors are described by the von Neumann neighborhood, which denotes that for $J = (i, j)$, $\mathcal{N}(J) = \{(i-1, j), (i+1, j), (i, j-1), (i, j+1)\}$. For $F = 0$, if an initial state contains one of the following patterns or their reflections

$$\begin{matrix} 1 & 2 \\ 0 & 0 \end{matrix} \quad , \quad \begin{matrix} 1 & 2 \\ 0 & 2 \end{matrix} \quad , \quad \begin{matrix} 1 & 1 \\ 2 & 0 \end{matrix} \tag{2}$$

then this pattern is persistent [26].

It can be proved that if $F = 0$ and $T \geq 3$, the system of the GH cellular automata becomes locally periodic with probability 1, and the period is T [25]. The proof is based on the idea of *a clock* — an invariant pattern which consists of a loop of sites along which all T states are arranged cyclically. Since $F = 0$, the state advances each time at every site of such a loop.

Thus no cells stay in state 0 for longer than 1 step. But if the lattice size is finite, we observe a transition (between the state driven by the SPO and the homogeneous pattern) as T — the length of the clock loop increases. See Fig. 2 (left) for rough estimates of T_{crit} obtained for $L = 100$, in the Moore neighborhood and with a different F.

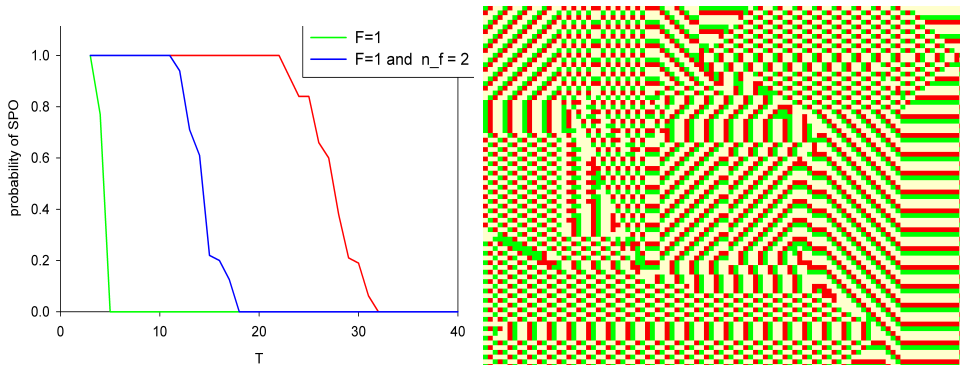

Fig. 2. Left: Probability of emergence of the SPO for different T. Simulation parameters: lattice 100×100, free boundary conditions, neighborhood consisting of 8 neighbors in the Moore neighborhood. Right: Example of an intriguing pattern emerging when $F = 1$ and $T = 4$.

When the threshold takes a value larger than 0, $F > 0$, it is much less clear whether a clock can be formed dynamically, and whether the limit pattern is locally periodic. For example, intriguing patterns are obtained if $F = 1$ and $T = 4$; see Fig. 2 (right). Thus the question about the transition in the ergodic behavior is governed by the question of the existence of the SPO.

In the probabilistic version of the GH model, the transition to firing (II) is governed by the transmission rate p_{T}. Berry and Fates in [27] considered properties of the probabilistic GH model for $F = 0$ and different neighborhoods on a square lattice. They found that the transition from a homogeneous limiting state to the SPO state is critical with respect to p_{T} and T. They provided arguments that this transition belongs to the universality class of directed percolation independently of the neighborhood shape and size. Directed percolation is a paradigm of transitions in nonequilibrium systems in which the transition point separates an active phase from a phase in which the dynamics is frozen (the so-called absorbing phase); see, *e.g.*, [28]. Belonging to the same universality class denotes that systems share the same critical properties. In particular, they have the same critical exponents of the basic state functions.

2.2. Sustained oscillations in GH automata distributed on stochastic square lattice

Let us assume that not all the connections to 8 neighbors in the Moore neighborhood are established. Let d describe the probability that there is a connection between the neighbors in the Moore neighborhood. Then $n(d) = 8d$ describes the mean number of nearest neighbors of a cell. It is obvious that the limit state will depend on d. In Fig. 3, we show examples of the limit patterns observed for different densities of neighbor connections n. Since the probability of establishing a clock decreases when n decreases, the limit patterns are constructed from fewer individual clocks. Moreover, patterns with periods different from T emerge; see cases $n = 3.2$ and $n = 2.4$ in Fig. 3. At very low densities, local stable patterns can be observed; see case $n = 2$ for len (refractory) $= 10$ in Fig. 3.

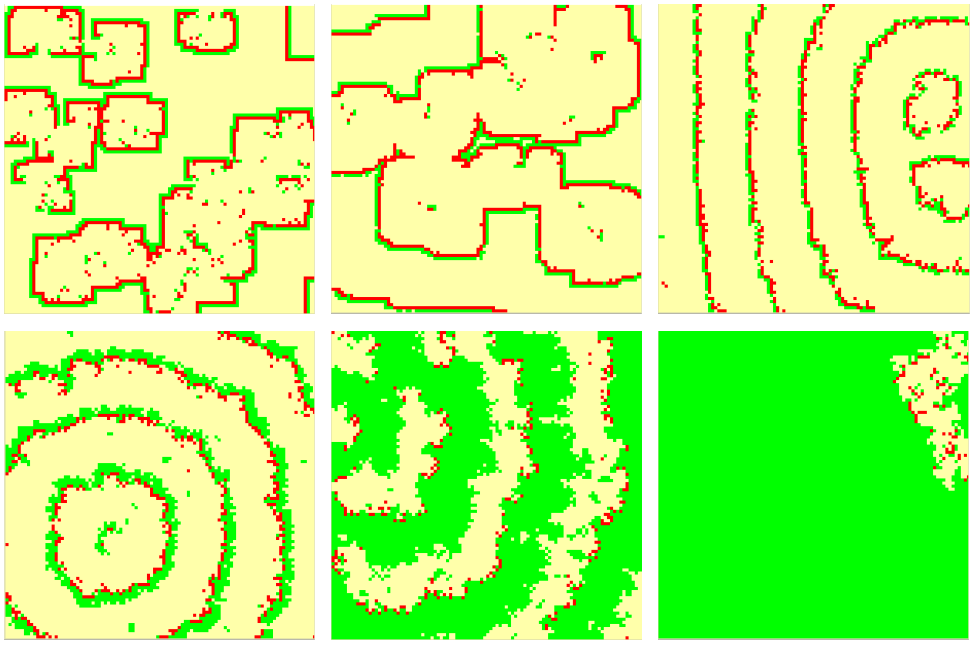

Fig. 3. Examples of SPO patterns obtained for $F > 0$, len (refractory) $= 15$ (hence $T = 17$) for the following numbers of random intercellular connections: (from the left to the right, from top to bottom) 8.0, 6.0, 4.0, 3.2, 2.4, 2.0.

Additionally, in Fig. 4 we present plots of critical changes in the probability of observing the SPO with different densities of neighbor connections with respect to the value of T.

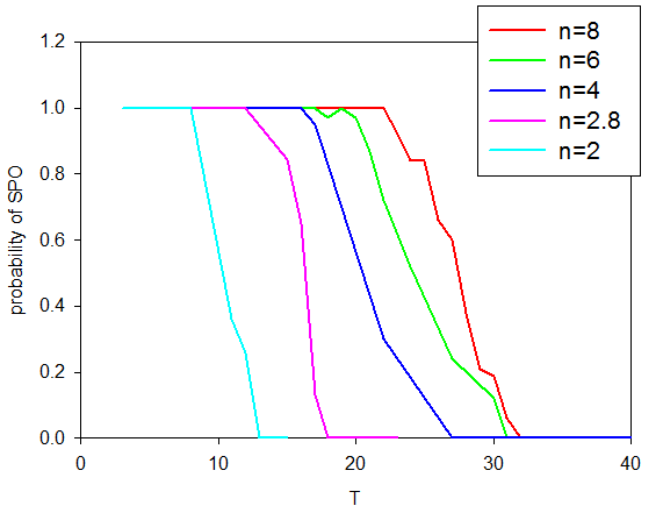

Fig. 4. Probability of observing the SPO in the limit state for different densities of intercellular connections when T is increasing.

Berry and Fates in [27] studied how defects in the topology of intercellular connection influence critical properties in the system. They considered both the missing cells and blocked connections. It occurs that independently of the intensity of defects, the system is critical with respect to p_{T} and this transition again belongs to the percolation universality class. By using mean-field tools, they were able to prove that the critical value for p_{T} relates to the mean number of the nearest neighbors inversely proportional to n, namely as $1/n$.

2.3. Elements of pacemaker physiology

In real pacemaker cells, the process of excitation, called depolarization of the cellular membrane, is due to calcium ions; see Fig. 5. The calcium ions are much heavier than the sodium ions which drive the depolarization in the cells of the working cardium. In consequence, the depolarization in the pacemaker cell progresses less rapidly than the depolarization in the myocytes in any other part.

It is known that the myocytes of the pacemaker are sparsely interconnected compared to the extent of interconnections observed in other tissues [29]. A typical pacemaker cell in the canine pacemaker is connected to only 4.8 ± 0.7 neighbors, compared with 11.3 ± 2.2 cells in the left ventricle and 6.4 ± 1.7 cells in the crista terminalis — the tissue propagating the excitation from the heart's first pacemaker — called the sinus node — to the

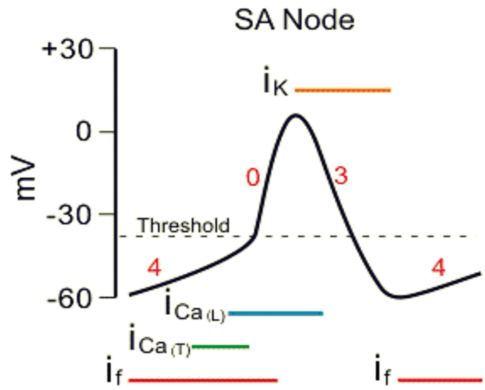

Fig. 5. Membrane potential of the pacemaker cell (diagram based on [18]). The membrane potential is negative due to the active transport driven by the molecular pumps (proteins embedded in the membrane), which change three sodium ions into two potassium ions. The depolarization process (marked as **0**) starts when the potential r reaches the threshold value. The change in the potential value is due to the inward calcium currents (denoted as $\boldsymbol{i}_{\mathrm{Ca(L)}}$). After the change in the membrane polarization, the potassium ions leave the cell, initiating the repolarization process (marked as **3**). Notice that the membrane potential does not remain constant after reaching the minimal value but slowly grows (marked as **4**). It is assumed that this growth is due to a so-called funny current $\boldsymbol{i}_{\mathrm{f}}$ — a mixture of the sodium and potassium ions.

heart's second pacemaker — called the atrial node. The intercellular connections of myocytes are based on intercalated disks — elaborate junctions of membranes at the cell's boundary. However, the aggregated junction profile length per unit myocyte area is 26.5 times greater in the left ventricle and 5.0 times greater in the crista terminalis than in the sinus node. This results in weaker interactions between the neighboring cells of the sinus node than between myocytes in the ventricle.

Additionally, the myocytes comprising the human sinus node are small when compared to the ventricle cell. They have poorly developed organelles, such as sacromeres and sacroplasmic reticulum, which enable cell contraction. They are organized in an irregularly bordered, highly fibrous connective tissue matrix. The high density of the connective tissue discriminates the nodal tissue from the surrounding non-nodal tissue [20].

In general, the connective tissue and fibroblasts form a structural support-framework for myocytes and blood vessels, guiding the cardiac tissue cytoarchitecture [30]. They contribute to structural, biochemical, mechanical and electrical properties of the myocardium. Cultured cardiac myocytes and fibroblasts readily form the functional gap junctions [31]. Fibroblasts

demonstrate long processes that envelope the myocytes. Fibroblasts can affect electrophysiology passively, for example by acting as obstacles to the spread of electrical excitation, or actively if they are coupled to myocytes. However, the collagen — protein produced by fibroblasts — separates small groups of cells from each other and thus limits the extent of intercellular contacts.

2.4. Pacemaker model based on GH cellular automata

Progress in biotechnological engineering allows the construction of cellular systems of myocytes. It is then possible to compare the electrochemical properties of such tissue with properties observed in cellular automata models. Bub, Shrier and Glass [32] constructed monolayers of cardiac cells of embryonic chickens, and compared properties obtained from the experiments with the results provided by the following cellular automata

$$\phi(t) : L \times L \to \{0, 1, \ldots, f, f+1, \ldots, f+r\} \tag{3}$$

that evolves according to the rules:
for $J \in L \times L$

(I) if $\phi(t, J) = \sigma \geq 1$, then $\phi(t+1, J) = (\sigma + 1) \bmod (f + r + 1)$;

(II) if $\phi(t, J) = 0$, then $\phi(t+1, J) = 1$

(a) if more than $F(t, J)$ neighbors of J are $1, \ldots, f$,

or

(b) with probability ρ.

Note that:

(a) In place of the firing step (coded as 1 in (3)), here we have a firing phase consisting of a sequence of states numbered from 1 to f. After completing the firing phase, a cell moves to the refractory phase.

(b) The excitation threshold $F(t, J)$ is assumed to depend on both t and the cell localization J. The first argument mimics the so-called fatigue effect of a cell that has just entered the activity state 0. Is it assumed that for a given cell, the threshold $F(t, J)$ for the transition to the state 1 lowers according to the length of the time t spent by the cell in the 0 state. The second argument is used to model the heterogeneity of intercellular connections. Bub, Shrier and Glass [32] move away from square lattice limitations with the idea proposed by Markus and Hess [33] to transform the integer coordinates of a square

lattice into real coordinates by adding a random component uniformly chosen from $[0, 1]$. This transformation allows the introduction of a more general cellular neighborhood than the neighborhood of nearest neighbors, namely all the cells located at a Euclidean distance less than some fixed value D from a cell are neighbors of this cell.

(c) Thanks to ρ in (II) (b), each cell performs self-excitation at random. However, in the simulation, this event is assumed to occur rarely $\rho = 0.001$, though it is known that pacemaker cells are self-excitatory.

This model reveals a crucial property observed in the natural system. The transition from spiral patterns, spontaneously initiated and terminated, to patterns with multiple fractionated wave fronts emerges if the density of cells and/or the strength of intercellular connections are changed [32]. This means that the cardiac tissue loses its functionality for impaired intercellular connections.

3. Synchronization in network automata

As described in Fig. 5, the cells of the sinus node perform identical, cyclically repeated steps. Thus, they are oscillating units rather than individuals quietly waiting for the next stimulation.

Intuitively, any oscillator $\boldsymbol{J}$ is a point moving on a circle of radius 1 with some angular velocity $\omega(J)$. If such oscillators are not coupled, the evolution of any oscillator $\boldsymbol{J}$ is

$$\phi(t, J) = \omega(J)t + \phi(0, J)\,, \tag{4}$$

where $\phi(0, J)$ is an initial phase of the oscillator $\boldsymbol{J}$.

Assuming that the oscillator remains in the basin of attraction of its limit cycle for a stimulus delivered at any phase in the cycle, one can describe the system by the set of phases $\phi(t, J)$ of the coupled oscillators [36]. The phase response curve is proposed as the function describing the change in the oscillator phase caused by the interaction. The phase can be pushed forward, or moved opposite to the direction of the free motion of the oscillator.

Several mathematical models have been proposed to study the spontaneous synchronization emerging in a system of coupled oscillators, spatially distributed in a network [8, 34]. The first solvable model was provided by Kuramoto [10]. The model is simple enough to be mathematically tractable, yet sufficiently complex to display a large variety of synchronization phenomena. Moreover, the model is sufficiently flexible to be adapted in many different contexts; see [11] for a review.

The Kuramoto model introduces the so-called Kuramoto order parameter K_Φ [10] to measure the phase synchronization of N oscillators

$$K_\phi = re^{i\Psi} = \frac{1}{N}\sum_{J=1}^{N} e^{i\phi(J)}\,. \tag{5}$$

If all oscillators are synchronized, *i.e.*, all have the same phase, then $|K_\Phi| = r = 1$. When all oscillators are completely out of phase with respect to each other, the value $|K_\Phi|$ remains close to 0 most of the time.

Among the coupled oscillators, a pulse-coupled network consisting of integrate-and-fire oscillators interacting with each other by impulse signals (*e.g.*, the Peskin model [37]) has been found as a prototype model for pacemaker cells of the heart [35], and therefore is characterized in more detail below.

3.1. Peskin model of coupling in oscillatory timed automata

Let us assume that a system of cells is a fully connected network of identical, pulse-coupled oscillators. Let the oscillator $\boldsymbol{J}$ evolve according to [37]

$$\dot{\phi}(t, J) = \Phi(0) - \gamma\phi(t, J)\,, \tag{6}$$

where $\Phi(0)$ and γ, with $\Phi(0) > |\gamma|$, and $\gamma \neq 0$, are intrinsic properties of the oscillator. If $\phi(t, J) = 1$, the oscillator $\boldsymbol{J}$ fires and $\phi(t, J)$ jumps back to 0.

Let the oscillators interact according to a rule:

$$\text{if } \phi(t, J) = 1 \text{ then } \phi\left(t^+, J'\right) = \min\left\{1, \phi\left(t, J'\right) + \varepsilon\right\} \text{ for each } \boldsymbol{J'} \neq \boldsymbol{J} \tag{7}$$

which means that when a given oscillator fires, it pulls all the other oscillators up by an amount ε, or pulls them up to firing, whichever is less.

Mirollo and Strogatz [35] proved that independently of how the system starts, the cells all end up firing in unison. Adapting the Peskin model to cellular automata, Bartocci *et al.* [23] used timed automata; see Fig. 6.

A timed automaton can be considered as the abstraction of a timed system. The timed automaton is a finite automaton (a graph containing a finite set of nodes and a finite set of labeled edges) extended within general real-valued variables [22]. These variables model the logical clocks in the system. They are initialized with the zero value when the system is started, and then their values increase synchronously at the same rate. Clock constraints, called guards, are introduced to restrict the behavior of the automaton. A transition, represented by an edge, can be made when the clock's values satisfy the guard that labels the edge. Clocks are often reset to zero when a transition is made.

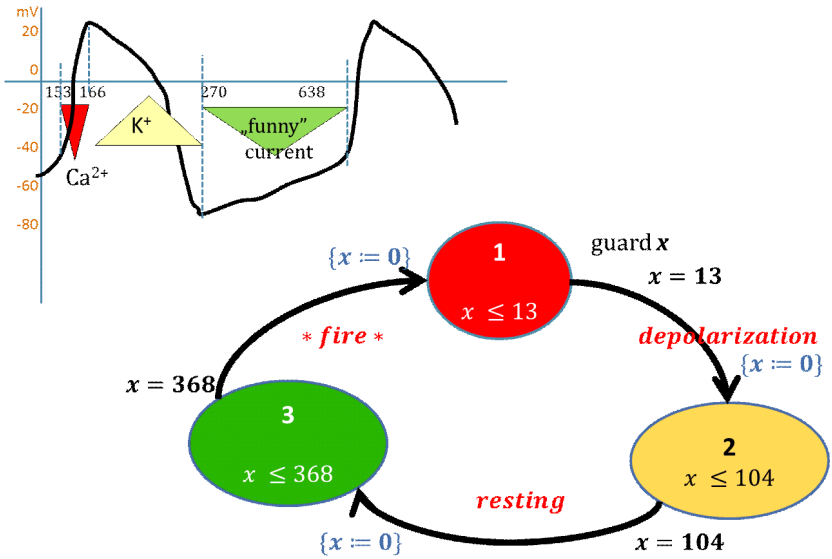

Fig. 6. Diagram explaining the oscillatory rule of Bartocci *et al.* applied to a timed automaton [23]. A clock, represented by the variable x, marks time spent by an automaton in each of the three states $\{1, 2, 3\}$. The transitions, called *depolarization*, *resting*, and *fire*, are guarded by the clock. The clock is reset after the transition. The special timing of the dynamics follows the characterization of the membrane potential of the rabbit pacemaker cell, which is shown in the top-left part of the diagram.

Bartocci *et al.* [23] have shown that 3 oscillatory timed automata, evolving in a way described in Fig. 6 and interacting according to the Peskin rule (7), achieve synchronization for some values of ϵ in the limit time.

4. The pacemaker automata network (PAN) model

The idea of the timed automata is used below to refine the pacemaker model previously studied by us [38–40].

4.1. Modeling heterogeneity of intercellular connections

Our proposition for remodeling of the square lattice connections corresponds to the algorithm designed by Watts and Strogatz [41] of rewiring network edges in a diffusive way, *i.e.* in a way in which each event of rewiring changes only one end of the edge. We modify this algorithm by inserting limits on how far the end of the rewired edge can diffuse; see Fig. 7, [38, 42]:

For each cell $J \in L \times L$ and for each link from J to any of J's neighbors $J' \in \mathcal{N}(J)$

(A) a connection from a cell J to a cell J' is broken with a probability dependent on the connectivity of the neighbor J', as follows

$$p_{\text{break}} = \frac{p}{\deg(J')}\,, \tag{8}$$

where $\deg(J')$ denotes degree of the node J';

(B) a new neighbor J'' for a cell J is chosen at random from the set of neighbors of J', so $J'' \in \mathcal{N}(J')$.

Exclusions: breaking the connection to a leaf is forbidden. (A leaf is a node which is of degree 1.)

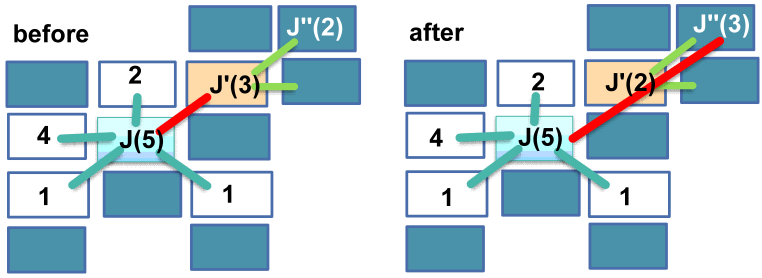

Fig. 7. Illustration of the rewiring algorithm. The $\boldsymbol{J}'$-end of the connection $(\boldsymbol{J}, \boldsymbol{J}')$ between cells $\boldsymbol{J}$ and $\boldsymbol{J}'$ is changed to $\boldsymbol{J}''$, which is the neighbor of cell $\boldsymbol{J}'$. $\boldsymbol{J}'$ is chosen at random but with the preference described by (8). $\boldsymbol{J}''$ is chosen at random from the neighbors of $\boldsymbol{J}'$. The numbers describe the actual vertex degree. Note that $\boldsymbol{J}$ has two neighbors of degree 1 — leaves — which, for the protection of the network connectivity, cannot be unlinked.

Note that all cells are considered in one remodeling step. Hence, each edge is considered twice: the first time as the connection from J to J', and the second time as the connection from J' to J. We call one remodeling step, one Monte Carlo (MC) step, and use the number of these steps as the measure of remodeling of the lattice. After each MC step, the table with the information about cell degrees is updated. If p is small enough, such remodeling mimics synchronized changes in the lattice [42]. By repeating the remodeling step many times, increasing numbers of cells that are distant on the square lattice metrics become neighbors.

The rewiring algorithm influences the distribution of vertex degrees; see Fig. 8. There appear vertices which have more than 8 neighbors. The more MC steps are applied, the more vertices with the high vertex degree appear. If a hundred MC steps are applied to a stochastic square lattice which initially has the mean number of nearest neighbors $\langle n \rangle = 4.5$, we obtain a network which has some cells connected to more than 10 cells. Hence, we can say the network is slightly heterogeneous.

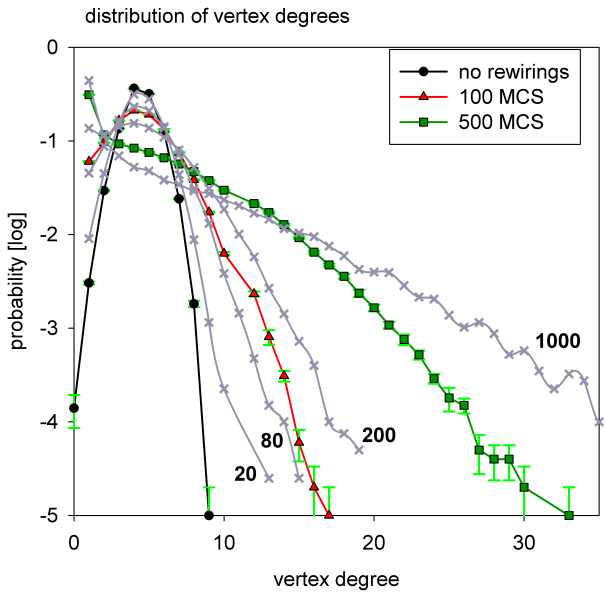

Fig. 8. Distribution of vertex degrees in a stochastic lattice with mean $n = 4.5$ transformed by the rewiring algorithm for different values of MC steps.

4.2. Model of a pacemaker automaton

Let $\phi(t, J, x)$ denote the 3-state timed automaton located in $J \in L \times L$.

Let the states of the automaton be $\sigma \in \{0 = \text{firing}, 1 = \text{refractory}, 2 = \text{activity}\}$.

Let x be the clock guarding transitions between states with thresholds $\theta(\sigma)$.

Then,

(I) if $\phi(t, J, x) = \sigma$ and $x < \theta(\sigma)$, then $\phi(t+1, J, x) = \sigma$ and $x = x+1$;

(I') if $\phi(t, J, x) = \sigma$ and $x = \theta(\sigma)$, then $\phi(t+1, J, x) = (\sigma + 1) \bmod 3$ and $x = 0$.

For illustration see Fig. 9.

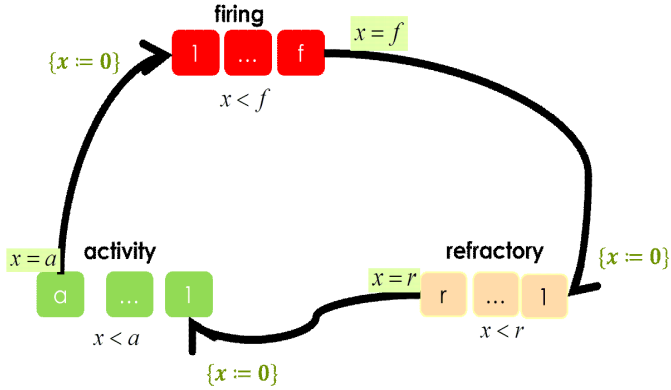

Fig. 9. Illustration of the intrinsic cycle of the pacemaker automaton. The three states of PA are called $\{firing, refractory, activity\}$. A clock, represented here by x variable, marks time spent by an automaton in each of these states. The transitions are guarded by the clock. After the transition, the clock is reset.

The rules (I) and (I') describe the free dynamics of the pacemaker automaton — a periodic sequence of length $\theta(0) + \theta(1) + \theta(2) = T$, of the automaton state and the corresponding clock count. Let us denote $f = \theta(0)$, $r = \theta(1)$, $a = \theta(2)$.

Then,

- the phase function, describing the advancement of the pacemaker automaton in its intrinsic cycle is defined as

$$\begin{aligned} \Phi[\phi(t,J,x)] \;=\; & x\delta_{0,\phi(t,J,x)} + [\theta(0)+x]\delta_{1,\phi(t,J,x)} \\ & + [\theta(0)+\theta(1)+x]\delta_{2,\phi(t,J,x)}\,. \end{aligned} \tag{9}$$

  In the case of the free evolution, the above formula can be simplified to

$$\Phi[\phi(t,J,x)] = [t \bmod T + \phi(0,J,x)] \bmod T;$$

- the pacemaker automaton is called *stochastic* if the clock x is allowed to jump into the guarding value of the actual automaton state with some probability s.

In the following, we limit the stochasticity of the clock guards to shortenings of the time elapsed by a cell in a given state. These shortenings are governed by the formula

$$x = \theta(\sigma) \text{ with probability } s = \left(1 - \frac{x}{\theta(\sigma)}\right)^{\xi} \text{ for } \xi \geq 0\,. \tag{10}$$

In this way, each automaton J performs the intrinsic cycle in a stochastic way with an actual set of the thresholds for transitions: $\theta(\sigma; J, x, t)$. Each time an automaton switches to the state 0, its phase Φ is reset to 0. Then Φ is advanced at each time step. Therefore, Φ measures time steps spent by the automaton in a given oscillation.

Let us assume that coupling between the pacemaker automata takes the form

(II) if $\phi(t, J, x) = 2$ and more than F neighbors of J are in the state 0, then $\phi(t+1, J, x) = 0$ and $x = 0$;

(II') if $\phi(t, J, x) = 1$ and more than R neighbors of J are in the 0, then $\phi(t+1, J, x) = 1$ and $x = \lfloor x/2 \rfloor$.

The coupling introduced by (II) leads to a reduction in the time steps which are spent by a cell in the *activity* state. This results in decreasing of the oscillation length. The coupling proposed by (II') shifts back the clock when a cell is in the *refractory* state. In consequence, an elongation of the cellular oscillation appears. Together these couplings establish the physiologically known system of the myocyte *activation* (II) — *inhibition* (II') [43].

Interactions (II) and (II') have a significantly different influence on the set of limit states. For example, when automata are located in vertices of a line and the evolution is deterministic, then the neighboring cells of the limit state have an oscillatory phase difference equal to 0 or to ± 1. Moreover, when rule (II') is turned off then the state with the phase difference equal to 0 is unstable. If rule (II') is activated, this state becomes attractive. Such a phase pattern denotes that all automata can go into the *firing* state at the same time. Therefore, they can be compared to a marching squad. This bifurcation occurs because of the property that for any two coupled cells, if the first cell is in state $(0, f)$ and the second cell is in state $(1, 1)$, in the next time step both these cells have the same state $(1, 1)$.

In situations other than that described above, we obtain [39]:

if a cell in the state **2** is a neighbor of a cell in the state **0**, then

$$\begin{pmatrix} (2,x) \\ (0,x') \end{pmatrix}_t = \begin{pmatrix} (0,1) \\ (0,x'+1) \end{pmatrix}_{t+1} = \ldots = \begin{pmatrix} (0,x) \\ (1,1) \end{pmatrix}_{t'} ;$$

if a cell in the state **1** is a neighbor of a cell in the state **0** then

$$\begin{pmatrix} (1,x) \\ (0,x') \end{pmatrix}_t = \begin{pmatrix} (1,x/2+1) \\ (0,x'+1) \end{pmatrix}_{t+1} = \ldots = \begin{pmatrix} (1,x'') \\ (1,1) \end{pmatrix}_{t'} \text{ with } x'' < x ;$$

if a cell in the state **1** is a neighbor of a cell in the state **1** and $x < x'$ then either:

$$\begin{pmatrix} (1,x) \\ (1,x') \end{pmatrix}_t = \ldots = \begin{pmatrix} (0,1) \\ (1,x'') \end{pmatrix}_{t'}$$

or

$$\begin{pmatrix} (1,x) \\ (1,x') \end{pmatrix}_t = \ldots = \begin{pmatrix} (0,1) \\ (2,x'') \end{pmatrix}_{t'} .$$

4.3. Physiological interpretation for the interaction driving parameters

The two parameters $\boldsymbol{F}$ and $\boldsymbol{R}$ which regulate the couplings (II) and (II') can be considered as measures of the sensitivity of a cell to the interactions of types (II) and (II'), correspondingly. Namely, a greater value of $\boldsymbol{F}$ means that more neighbors in the *firing* state are required to cause the excitation of a cell. Similarly, a greater value of $\boldsymbol{R}$ means that more neighbors in the *firing* state must be present to elongate the cellular cycle.

Taking into account the features of the nodal tissue described in the previous section, we can enumerate the two settings of the coupling parameters as physiologically relevant:

- $\boldsymbol{F} > 0$ and different $\boldsymbol{R}$ values as revealing the *excitable tissue* because this setting describes the tissue which is sensitive to signal propagation;
- $\boldsymbol{F} > 1$ and different $\boldsymbol{R}$ values as revealing the *pacemaker tissue* because this setting reflects a smaller area of intercellular junctions in the sinus nod tissue than the junctional area among the ventricular cells, which, in consequence, requires more neighbors in the *firing* state to reach the threshold for interactions.

4.4. Synchronization in PAN

In general, the pattern formation is the visible outcome of the self-organization process; see Fig. 10. When we search for the pacemaker functionality, we expect the emergence of the center which produces the sustained oscillations propagating to the system boundary. It appears that depending on the density of intercellular connections, one or more such centers can develop. However, intercellular interactions of type (II') have the tendency to stabilize the system with all automata marching as a squad. Therefore, the automatic classification of the stationary patterns might be ambiguous.

We took up the challenge to classify the stationary patterns in the three main groups: collapsing circular patterns, expanding circular patterns and marching squad patterns [39]. However, in some cases, one can obtain a mixture of these classes. In Fig. 11, we show the dependence on the probability

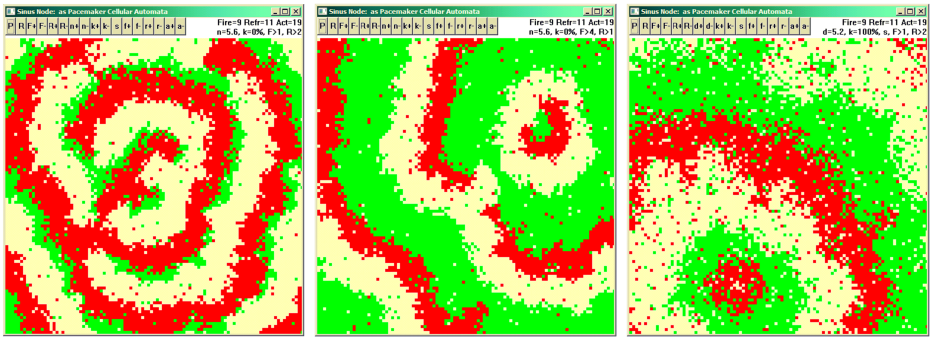

Fig. 10. Typical patterns in the stationary states obtained in networks of the pacemaker automata self-organized to the common oscillation. All the patterns are obtained for the same density of intercellular connections $n = 5.6$, but for a different sensitivity of interactions and/or different network structure. Left: $\boldsymbol{F} > 1, \boldsymbol{R} > 2$, the rule is deterministic, the network is homogeneous. The limit pattern is made of the expanding circular fronts. Middle: $\boldsymbol{F} > 4, \boldsymbol{R} > 1$, the rule is deterministic, the network is homogeneous. The limit pattern is built from the collapsing circular fronts. Right: $\boldsymbol{F} > 1, \boldsymbol{R} > 2$, the rule is stochastic, the network is rewired 100 MCS. The limit pattern presents the strong and fast-moving front of the expanding excitation.

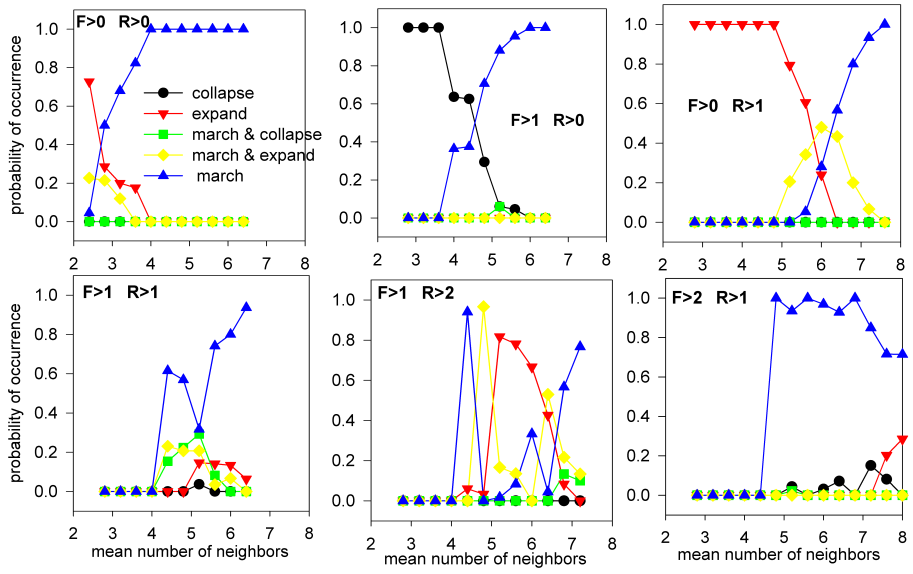

Fig. 11. Probability of encountering the stationary pattern as collapsing, expanding or marching as a squad for different sensitivities of interactions and different densities of intercellular connections.

of occurrence of the particular classes with respect to the mean number of neighbors n. The plots, in particular, refer to the deterministic pacemaker automata arranged on a homogeneous stochastic network. It appears that the largest variety of the possible outcomes is when $\boldsymbol{F} > 1, \boldsymbol{R} > 1$ or $\boldsymbol{F} > 1, \boldsymbol{R} > 2$, and for a density of neighbors of four to six. We claim that these parameters describe the cardiac pacemaker properties.

The Kuramoto parameter K_{Φ}, defined in (5), is perfectly suited to detecting patterns of a marching squad because $K_{\Phi} = 1$ in these patterns. Therefore, by observing conditions when K_{Φ} changes from that value, we can automate the classification of the stationary patterns.

In order to get K_{Φ}, two groups of computer experiments were performed. In the experiments in the first group, we investigated properties of K_{Φ} obtained for deterministic pacemaker automata distributed on the homogeneous stochastic networks; see Fig. 12. The second group of simulations was concentrated on properties of the stochastic pacemaker automata, with $\xi = 10$ (see (10)), which were located on the network with edges rewired 100 MCS; see Fig. 13.

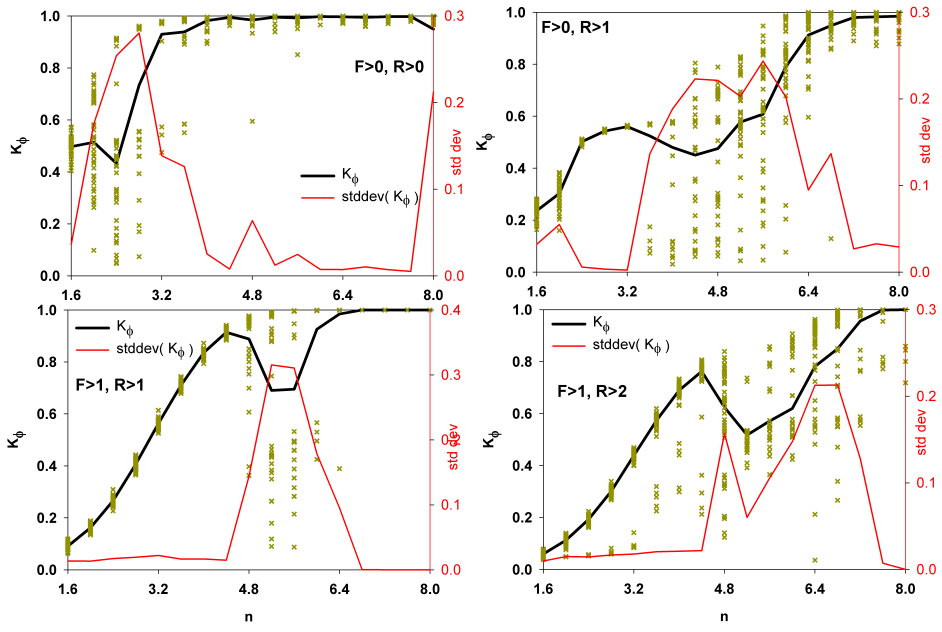

Fig. 12. Mean Kuramoto order parameter K_{Φ} obtained in experiments with the deterministic pacemaker automata located on the homogeneous network for different densities of intercellular connections $\boldsymbol{n}$ and different values of the sensitivity parameters $\boldsymbol{F}$ and $\boldsymbol{R}$ for interactions. The grey/green marks show all results obtained. The thin/red curves are standard deviations of the results.

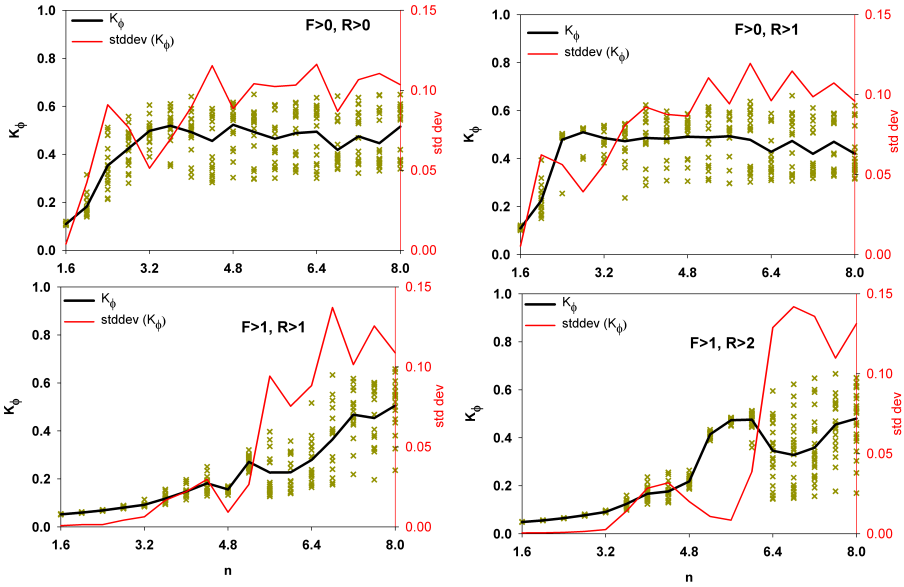

Fig. 13. Mean Kuramoto order parameter K_Φ obtained in experiments with the stochastic pacemaker automata located on the rewired 100MCS networks for different densities of intercellular connections $\boldsymbol{n}$ and different values of the sensitivity parameters $\boldsymbol{F}$ and $\boldsymbol{R}$ for interactions. The grey/green marks show all the results obtained. The thin/red curves are standard deviations of the results.

Each group of experiments consisted of either 50 (deterministic rule) or 30 (stochastic rule) independent simulations, which were performed for different densities n of intercellular connections. The lattice size was $L = 100$, which means that $N = 10^4$ interacting cells were considered. Free boundary conditions were assumed. The initial state in all the experiments was the primordial soup. The thresholds for the transitions to the next cellular state were $f = 9$, $r = 11$, $a = 19$. In each experiment, the first 10^4 steps were not included in the analysis. Then the states were assumed to be stationary, and the statistics of K_Φ were recorded.

We can learn from Fig. 12 that deterministic pacemaker automata evolving with stochastic but homogeneous networks of intercellular connections, led to patterns of the marching squad type. However, if the density of the intercellular connections is $n \in (4.5, 6)$, other stable solutions emerge. These solutions can be described as patterns with a huge variety of circular waves.

In contrast, if the pacemaker system is built from stochastic pacemaker automata distributed on rewired networks (though the intercellular connections are slightly heterogeneous), the marching squad synchronization does not emerge for any model parameters significant for the cardiac pacemaker modeling; see Fig. 13. Additionally, we can see that for densities $n \in (4.5, 6)$,

when the sensitivity parameters $\boldsymbol{F} > 1$, $\boldsymbol{R} > 2$ correspond to the cardiac pacemaker, the variety of solutions is rather restricted. This is the case when patterns of the type shown in the last panel of Fig. 11 occur with high probability.

4.5. Sinus node aging via pacemaker network automata

It is known that the function of the sinus node declines with age, leading to the condition called *sick sinus syndrome* [44]. This syndrome is basically associated with a variety of cardiac arrhythmia or conduction disturbances [45]. Sick sinus syndrome accounts for more than 50% of pacemaker implantations in people over 60 years of age.

The sinus node function impairment may occur (a) as a result of structural changes (collagen deposition), (b) as alterations in the ion channels (the expression and/or the function of ion channels may be perturbed), or (c) as impairment in cell-to-cell communication (altered gap junction). All of the changes above can be easily reconstructed in the considered model of the PAN. Subsequently, (a) an increase in the collagen deposition can be modeled as a decrease in the density of intercellular connections; (b) and (c) changes in the performance of the ion channels can be encoded as different timings in the pacemaker automaton cycles or via parameters $\boldsymbol{F}$, and $\boldsymbol{R}$ measuring the sensitivity of interactions.

Furthermore, the membrane potential is used in experiments as the outcome of the changes in the expression of genes responsible for the performance of ion channels [19, 20, 45]. For example, the expression of genes of $\mathrm{Ca}_\nu 1.2$, $\mathrm{Ca}_\nu 1,3$ channels, which are responsible for the $\boldsymbol{I}_{\mathrm{CaL}}$ current (see Fig. 5), is measured by the speed of the fast depolarization. In this way, the length of the fast depolarization — via threshold value f for the clock guarding the *firing* state — provides inter-scale insight into the role of particular processes in the functionality of the pacemaker. Similarly, the activity of the potassium channels: $\mathrm{K}_\nu 4.2$, $\mathrm{K}_\nu 4.3$, *etc.* (see [20] for a more complete list), which are responsible for $\boldsymbol{I}_{\mathrm{K}}$ for the repolarization of the membrane potential, can be evaluated by the time in which the membrane reactivates its lowest potential.

Though the PAN model is based on macroscopic properties of the features of the membrane of the sinus node myocyte, and therefore the behavior of cellular ion channels and currents cannot be directly taken into account, indirectly even changes in the expression of genes can be included.

5. Conclusions

Systems biology is a multidisciplinary field, the goal of which is to provide an integrative level of understanding of biological systems [15]. Systems biology could greatly benefit from the development of abstraction techniques

that, given a system of experimental results, construct a more abstract model in which the properties of interest are preserved. The technique presented of timed automata having a complex network of interactions is promising because it replaces the properties of transient behaviors, which are intuitively and commonly acceptable, with discrete transitions. The heterogeneous nature of the considered network structure and the stochasticity of the automata cycle appear fundamental in reproducing the propagation behavior of curvilinear fronts. Both these properties provide conditions for the development of stable leading pacemaker oscillations.

However, there are always complaints that discrete models present systems in an oversimplified way that is far from the solution of real problems. Nevertheless, thanks to discrete models' simplicity in design and comprehensibility, these models allow for a significant advance in our understanding, and provide insight into how to process multiscale dynamical systems. Our personal enthusiasm for discrete modeling is greatly strengthened by the fact that discrete modeling is the only way in which complex phenomena can be efficiently simulated on commercial computers.

This research was supported by the Polish National Science Centre UMO: 2012/06/ M/ST2/00480.

REFERENCES

[1] G. Grinstein, C. Jayaprakash, Yu He, *Phys. Rev. Lett.* **55**, 2527 (1985).
[2] J.L. Lebowitz, C. Maes, E.R. Speer, *J. Stat. Phys.* **59**, 117 (1990).
[3] D. Makowiec, *Phys. Rev.* **E55**, 6582 (1997).
[4] P. Bak, Ch. Tang, K. Wiesenfeld, *Phys. Rev. Lett.* **59**, 381 (1987).
[5] K. Nagel, M. Schreckenberg, *Journal de Physique I* **2**, 2221 (1992).
[6] D. Stauffer, *Adv. Complex Systems* **4**, 19 (2001).
[7] D. Makowiec, *Physica A* **344**, 36 (2004).
[8] A. Pikovsky, M. Rosenblum, J. Kurths, *Synchronization. A Universal Concept in Nonlinear Science*, Cambridge University Press, UK, 2001.
[9] J.M. Greenberg, S.P. Hastings, *SIAM J. Appl. Math.* **34**, 515 (1978).
[10] Y. Kuramoto, *Chemical Oscillations, Waves and Turbulence*, Springer, Berlin, 1984.
[11] J.A. Acebron *et al.*, *Rev. Mod. Phys.* **77**, 137 (2005).
[12] P. Ye, E. Entcheva, S.A. Smolka, in: Proceedings of Computational Methods in Systems Biology, 2005, pp. 216–227.
[13] A.L. Hodgkin, A.F. Huxley, *J. Physiol.* **117**, 500 (1952).
[14] C.H. Luo, Y. Rudy, *Circulation Research* **68**, 1501 (1991).

[15] H. Kitano, *Nature* **420**, 206 (2002).

[16] M. Stumpf, D.J. Balding, M. Gorolami, *Handbook of Statistical Systems Biology*, Wiley, 2011.

[17] J. Jalife *et al.*, *Basic Cardiac Electrophysiology for the Clinician*, Wiley-Blackwell, 2002.

[18] R.E. Klabunde, Cardiovascular Physiology Concepts, accessible via `http://www.cvphysiology.com/Arrhythmias/A005.htm`

[19] M.E. Mangoni, J. Nargeot, *Physiol. Rev.* **88**, 919 (2008).

[20] O. Monfredi *et al.*, *PACE* **33**, 1392 (2010).

[21] A. Rose, *Exp. Physiol.* **96**, 1114 (2011).

[22] R. Alur, D.L. Dill, *Theor. Comp. Science* **126**, 183 (1994).

[23] E. Bartocci, F. Corradini, E. Merelli, L. Tesei, *Theor. Comp. Science* **411**, 1999 (2010).

[24] R. Fisch, J. Gravner, D. Griffeath, *Stat. Comput.* **1**, 23 (1991).

[25] R. Durrett, D. Griffeath, *Experimental Math.* **2**, 183 (1993).

[26] J.M. Greenberg, C. Greene, S.P. Hastings, *Int. J. Unconventional Comp.* **1**, 399 (2005).

[27] H. Berry, N. Fates, *Int. J. Unconventional Comp.* **7**, 65 (2011).

[28] G. Odor, *Rev. Mod. Phys.* **76**, 663 (2004).

[29] J.E. Saffitz, D.L. Lerner, K.A. Yamada, in *Cardiac Electrophysiology. From Cell to Bedside*, D.P. Zipes, J. Jalive (Eds.), Saunders Co., Philadelphia, PA USA, 2004, pp. 181–191.

[30] P. Camellitti, T.K. Borg, P. Kohl, *Cardiovasc. Res.* **65**, 40 (2005).

[31] M.B. Rook, H.J. Jongsma, B. de Jonge, *Pflügers Arch.* **414**, 95 (1989).

[32] G. Bub, A. Shrier, L. Glass, *Phys. Rev. Lett.* **94**, 028105 (2005).

[33] M. Markus, B. Hess, *Nature* **347**, 56 (1990).

[34] A. Arenas *et al.*, *Phys. Rep.* **469**, 93 (2008).

[35] R.E. Mirollo, S.H. Strogatz, *SIAM J. Appl. Math.* **50**, 1645 (1990).

[36] A.T. Winfree, *Biomathematics* **8**, Springer-Verlag, New York 1980.

[37] C.S. Peskin, *Courant Institute of Mathematical Sciences*, 1975.

[38] D. Makowiec, *Int. J. Mod. Phys.* **C21**, 107 (2010).

[39] D. Makowiec, *Acta Phys. Pol. B Proc. Suppl.* **5**, 85 (2012).

[40] D. Makowiec, *Lecture Notes Comp. Sci.* **7956**, 138 (2013).

[41] D.J. Watts, S.H. Strogatz, *Nature* **393**, 409 (1998).

[42] D. Makowiec, *Eur. Phys. J.* **B48**, 547 (2005).

[43] A.C.F. Coster, B.G. Cellar, *Ann. Biomedical Engineering* **31**, 271 (2003).

[44] M.R. Boyett, *Experimental Physiol.* **94**, 1035 (2009).

[45] H. Dobrzynski, M.R. Boyett, R.H. Anderson, *Circulation* **115**, 1921 (2007).